



HAL
open science

Set inversion under functional uncertainties with Gaussian Process Regression defined in the joint space of control and uncertain

Reda El Amri, Céline Helbert, Miguel Munoz Zuniga, Clémentine Prieur,
Delphine Sinoquet

► To cite this version:

Reda El Amri, Céline Helbert, Miguel Munoz Zuniga, Clémentine Prieur, Delphine Sinoquet. Set inversion under functional uncertainties with Gaussian Process Regression defined in the joint space of control and uncertain. 2021. hal-02986558v2

HAL Id: hal-02986558

<https://ifp.hal.science/hal-02986558v2>

Preprint submitted on 30 Sep 2021 (v2), last revised 20 Jul 2023 (v5)

HAL is a multi-disciplinary open access archive for the deposit and dissemination of scientific research documents, whether they are published or not. The documents may come from teaching and research institutions in France or abroad, or from public or private research centers.

L'archive ouverte pluridisciplinaire **HAL**, est destinée au dépôt et à la diffusion de documents scientifiques de niveau recherche, publiés ou non, émanant des établissements d'enseignement et de recherche français ou étrangers, des laboratoires publics ou privés.

Set inversion under functional uncertainties with Gaussian Process Regression defined in the joint space of control and uncertain variables

Mohamed Reda El Amri^{a,*}, Céline Helbert^b, Miguel Munoz Zuniga^c, Clémentine Prieur^d,
Delphine Sinoquet^c

^aFormerly IFP Energies Nouvelles, Rueil-Malmaison, France.

^bECL, ICJ, UMR 5208, Université de Lyon, 36 av. G. de Collongue, Ecully, France.

^cIFP Energies Nouvelles, Rueil-Malmaison, France.

^dUniv. Grenoble Alpes, CNRS, Inria, Grenoble INP, LJK, Grenoble, France.

Abstract

In this paper we propose an efficient sampling strategy to solve an inversion problem subjected to functional uncertainties. More precisely, we aim at characterizing a control variable region defined by exceedance above a prescribed threshold of specific Quantities of Interest (QoI). This study is motivated by an automotive industrial application consisting in the identification of the set of values of control variables of a gas after-treatment device, in line with pollutant emission standards of a vehicle under driving profile uncertainties. In that context, driving profile uncertainties are modelled by a functional random variable and the constrained response in the inversion problem is formulated as the expectation over this functional random variable only known through a set of realizations. As often in industrial applications, this problem involves time-consuming computational models. We thus propose an approach that uses Gaussian Process meta-models built on the joint space of control and uncertain input variables. Specifically, we define a learning criterion based on uncertainty in the excursion of the Gaussian Process and derive tractable expressions for variance reduction in such a framework. Applications to analytical examples, followed by the automotive industrial test case show the accuracy and the efficiency brought by the procedure we propose.

Keywords: Set inversion; Gaussian Process meta-models; Data reduction; Functional uncertainties.

1. Introduction

In recent years, engineers and scientists are increasingly relying on computer models as surrogate for physical experimentation generally too costly or impossible to execute ([BGL⁺12, CBG⁺14]). In particular, practitioners using these numerical simulations are not only interested in the response of their model for a given set of inputs (forward problem) but also in recovering the set of input values leading to a prescribed value or range for the output of interest. The problem of estimating such a set is called hereafter an inversion problem.

In our context, the numerical simulator modelling the system, denoted f , takes two types of input variables: a set of control variables $\mathbf{x} \in \mathbb{X}$, and a set of uncertain variables $\mathbf{v} \in \mathcal{V}$. With-

*Corresponding author

Email address: elamri.reda@yahoo.com (Mohamed Reda El Amri)

out considering any assumptions on the distribution of the uncertain variable \mathbf{v} , robust inversion consists in seeking the set of control variables $\mathbf{x} \in \mathbb{X}$ such that $\sup_{\mathbf{v} \in \mathcal{V}} f(\mathbf{x}, \mathbf{v})$ is smaller than a threshold c . Then, the difficulty of solving the robust inversion problem strongly depends on the uncertainty set \mathcal{V} . In our setting, \mathcal{V} is a functional space, and we consider the inversion problem under uncertainty as a stochastic inversion problem, assuming that the uncertainty has a probabilistic description. Let \mathbf{V} denote the associated random variable, valued in \mathcal{V} , modelling the uncertainty. In our framework, we are interested in recovering the set $\Gamma^* := \{\mathbf{x} \in \mathbb{X}, g(\mathbf{x}) = \mathbb{E}_{\mathbf{V}}[f(\mathbf{x}, \mathbf{V})] \leq c\}$, with $c \in \mathbb{R}$, and the functional random variable \mathbf{V} is only known from a set of realizations. The expectation appearing in Γ^* has to be estimated. Moreover, the simulations are time consuming and thus the usual Monte Carlo method to estimate the expectation ought to be avoided.

Inversion problems have already been carried out in many applications, notably reliability engineering (see, e.g., [BGL⁺12], [CBG⁺14]), climatology (see, e.g., [BL15], [FS⁺13]) and many other fields. In the literature, one way to solve the problem is to adopt a sequential sampling strategy based on a Gaussian Process (GP) emulator of $g : \mathbf{x} \mapsto \mathbb{E}_{\mathbf{V}}[f(\mathbf{x}, \mathbf{V})]$. The underlying idea is that Gaussian Process emulators, which capture prior knowledge about the regularity of the unknown function, make it possible to assess the uncertainty about Γ^* given a set of evaluations of g . More specifically, for the estimation of an excursion set, these sequential strategies are closely related to the field of Bayesian global optimization (see, e.g., [CG13]). In the case of inversion problems, Stepwise Uncertainty Reduction (SUR) strategies based on set measures were introduced in [VB09]. More recently, a parallel implementation of these strategies has been proposed in [CBG⁺14] and applied to the recovery of an excursion set. Briefly, the strategy SUR gives sequentially the next location in the control space where to run the simulator in order to minimize an uncertainty measure of the excursion set.

In the field of robust optimization where uncertainty comes from a real-valued (or vector-valued) random input, various methods exist and aim at optimizing the expectation taken with respect to the probability distribution of the random input (see [JLR13] or [WSN00]). These methods are based on the modelling of f by a Gaussian Process built in the joint space of deterministic and uncertain variables. Then a "projected" (integrated) Gaussian Process is defined by taking the expectation with respect to the probability distribution of the random input, leading to an approximation of the expected response g . Finally an adaptive design of experiments (DoE) is proposed for optimizing the objective function g .

In the same spirit, we propose an original method to deal with a stochastic inversion problem with the aim of reducing the number of simulations required. In this work f is approximated by a Gaussian Process model built on the joint space $\mathbb{X} \times \mathcal{V}$. For the iterative approximation of Γ^* , the sampling strategy in the joint space is based on two steps. Firstly a SUR approach is applied to the "projected" Gaussian Process to determine the next evaluation point $\mathbf{x}_{n+1} \in \mathbb{X}$. Secondly, in the uncertain space, the next function v_{n+1} is chosen such that the standard error of the "projected" process evaluated at \mathbf{x}_{n+1} is minimized. It is important to note that our study is driven by an industrial test case on automotive depollution. More precisely, we study an after-treatment device of diesel vehicles, depending on control variables, in an uncertain environment corresponding to the uncertain driving profile. Knowledge on the driving profile is provided through a finite set of realizations of moderate size (see Section 4.4 for more details). In the following, we thus restrict our study to this setting: the knowledge on the uncertain functional input is limited to a finite set of realizations. Compared to methods based on an accurate estimation of the expectation and the construction of a surrogate of g ([EAHL⁺20]) our adaptive design of experiments, defined in the joint space, leads to further reduce the number of calls to the numerical simulator.

The article is structured as follows. Firstly, in Section 2, we recall the problem formulation and we extend the concept of Gaussian Process modelling to the case where the inputs contain a functional variable known only through a finite set of realizations. In Section 3, we introduce a new adaptive sampling strategy to choose the next point in the joint space: $(\mathbf{x}_n, \mathbf{v}_n)$, which reduces the most the uncertainty on the desired inversion set. The whole algorithm for our robust inversion procedure is then detailed. In Section 4, our procedure is implemented on two analytical test cases (Sections 4.1 and 4.2), and the modelling assumptions are discussed (Section 4.3). Concerning the uncertain space, we compare our sampling strategy, based on the standard deviation of the "projected" process evaluated at \mathbf{x}_{n+1} , with a uniform sampling of the next function v_{n+1} . We also compare our resolution procedure of a stochastic inversion problem with the one introduced in [EAHL⁺20] which combines the fitting of a Gaussian Process model on the control space \mathbb{X} with a quantization estimation of the expectation in the uncertain space \mathcal{V} . Finally, our new procedure is tested on the industrial test case of a car pollution control system (Section 4.4).

2. Problem formulation

We model the output of the industrial simulator by a function $f : \mathbb{X} \times \mathcal{V} \rightarrow \mathbb{R}$ with \mathbb{X} the space of control variables a bounded subset of \mathbb{R}^p and \mathcal{V} the space of the functional uncertain input. We model the functional uncertain input by a random variable \mathbf{V} valued in \mathcal{V} . We are interested in estimating the set

$$\Gamma^* = \{\mathbf{x} \in \mathbb{X}, g(\mathbf{x}) \leq c\}, \quad (1)$$

where $c \in \mathbb{R}$ is a threshold and $g : \mathbb{X} \rightarrow \mathbb{R}$ such that $g(\mathbf{x}) = \mathbb{E}_{\mathbf{V}}[f(\mathbf{x}, \mathbf{V})]$. An additional constraint is that \mathbf{V} is known only through a finite set of realizations. The implication of this constraint will be specified in Section 3.3.

The proposed sequential strategy to approximate Γ^* involves two main ingredients introduced hereafter : functional data reduction to reduce the uncertain space to a finite dimensional space and Gaussian Process modelling in the joint space *Control* \times *Uncertain*.

2.1. Functional data reduction

Let $(\Omega, \mathcal{F}, \mathbb{P})$ be a probability space. We assume that the random process \mathbf{V} belongs to $\mathcal{H} = \mathbb{L}^2(\Omega, \mathcal{F}, \mathbb{P}; \mathcal{V})$ with

$$\mathcal{V} = \left\{ \mathbf{v} : [0, T] \rightarrow \mathbb{R}, \|\mathbf{v}\| = (\langle v, v \rangle)^{1/2} = \left(\int_0^T \mathbf{v}(t)^2 dt \right)^{1/2} < +\infty \right\}.$$

We assume that $\mathbf{V} \in \mathcal{H}$ has zero mean and continuous covariance function $C(t, s)$. Then

$$\mathbf{V}(t) = \sum_{i=1}^{\infty} U_i \psi_i(t), \quad t \in [0, T], \quad (2)$$

where $\{\psi_i\}_{i=1}^{\infty}$ is an orthonormal basis of eigenfunctions of the integral operator corresponding to C such that:

$$\lambda_i \psi_i(t) = \int_0^T C(t, s) \psi_i(s) ds, \quad (3)$$

and with $\{U_i\}_{i=1}^{\infty}$ denoting a set of uncorrelated random variables with zero mean and variance λ_i . Decomposition (2) is known as the Karhunen-Loève (KL) expansion of \mathbf{V} ([LK10]). In the

following we denote the truncated version of \mathbf{V}

$$\mathbf{V}_m(t) = \sum_{i=1}^m U_i \psi_i(t), \quad (4)$$

which represents, in the mean square error sense, the optimal m -term approximation of \mathbf{V} ([LK10]). The value of the parameter m should be chosen such that the approximation is accurate enough. Its influence in practice is discussed in Section 4.2.

2.2. Gaussian Process modelling

We assume that $f(\mathbf{x}, \mathbf{v})$ is a realization of a Gaussian Process $Z_{(\mathbf{x}, \mathbf{u})}$ defined on $\mathbb{X} \times \mathbb{R}^m$, where $\mathbf{u} = (\langle \mathbf{v}, \psi_1 \rangle, \dots, \langle \mathbf{v}, \psi_m \rangle)^\top$.

Let m_Z be the mean function of $Z_{(\mathbf{x}, \mathbf{u})}$ and k_Z its covariance function,

$$\begin{aligned} \mathbb{E}[Z_{(\mathbf{x}, \mathbf{u})}] &= m_Z(\mathbf{x}, \mathbf{u}), \\ \text{Cov}(Z_{(\mathbf{x}, \mathbf{u})}, Z_{(\mathbf{x}', \mathbf{u}')} &= k_Z(\mathbf{x}, \mathbf{u}; \mathbf{x}', \mathbf{u}'). \end{aligned} \quad (5)$$

Let us denote Z^n , the GP Z conditioned on the set of n observations (simulations) $\mathbf{Z}_n = \{f(\mathbf{x}_1, \mathbf{v}_1), \dots, f(\mathbf{x}_n, \mathbf{v}_n)\}$ of Z at $\mathcal{X}_n \times \mathcal{U}_n = \{(\mathbf{x}_1, \mathbf{u}_1), \dots, (\mathbf{x}_n, \mathbf{u}_n)\}$ where $\mathbf{u}_i = (\langle \mathbf{v}_i, \psi_1 \rangle, \dots, \langle \mathbf{v}_i, \psi_m \rangle)^\top$

$$Z_{(\mathbf{x}, \mathbf{u})}^n = [Z_{(\mathbf{x}, \mathbf{u})} | Z_{\mathcal{X}_n \times \mathcal{U}_n} = \mathbf{Z}_n]. \quad (6)$$

The conditional expectation is

$$\mathbb{E}[Z_{(\mathbf{x}, \mathbf{u})}^n] = m_Z(\mathbf{x}, \mathbf{u}) + k_Z((\mathbf{x}, \mathbf{u}); \mathcal{X}_n \times \mathcal{U}_n) k_Z(\mathcal{X}_n \times \mathcal{U}_n; \mathcal{X}_n \times \mathcal{U}_n)^{-1} (\mathbf{Z} - m_Z(\mathcal{X}_n \times \mathcal{U}_n)),$$

and the conditional covariance is

$$\begin{aligned} \text{Cov}(Z_{(\mathbf{x}, \mathbf{u})}^n, Z_{(\mathbf{x}', \mathbf{u}')}^n) &= k_Z((\mathbf{x}, \mathbf{u}); (\mathbf{x}', \mathbf{u}')) \\ &\quad - k_Z((\mathbf{x}, \mathbf{u}); \mathcal{X}_n \times \mathcal{U}_n) k_Z(\mathcal{X}_n \times \mathcal{U}_n; \mathcal{X}_n \times \mathcal{U}_n)^{-1} k_Z(\mathcal{X}_n \times \mathcal{U}_n; (\mathbf{x}', \mathbf{u}')). \end{aligned}$$

It is important to note that the Gaussian Process $Z_{(\mathbf{x}, \mathbf{u})}$ is defined on the finite-dimensional truncated space $\mathbb{X} \times \mathbb{R}^m$. A discussion about this model is proposed in Section 4.3.

2.3. Integrated Gaussian Process

Recall that $\Gamma^* = \{\mathbf{x} \in \mathbb{X}, g(\mathbf{x}) = \mathbb{E}[f(\mathbf{x}, \mathbf{V})] \leq c\}$. Therefore, to model the function g , we introduce the integrated process

$$Y_{\mathbf{x}}^n = \mathbb{E}_{\mathbf{U}}[Z_{(\mathbf{x}, \mathbf{U})}^n] = \int_{\mathbb{R}^m} Z_{(\mathbf{x}, \mathbf{u})}^n d\rho(\mathbf{u}), \quad (7)$$

where $d\rho(u)$ is the probability distribution of $\mathbf{U} = (U_1, \dots, U_m)^T$ introduced in (4). The process $Y_{\mathbf{x}}^n$ is a Gaussian Process ([JLR13]) fully characterized by its mean and covariance functions which are given by

$$\begin{aligned} \mathbb{E}[Y_{\mathbf{x}}^n] &= \int_{\mathbb{R}^m} m_Z(\mathbf{x}, \mathbf{u}) d\rho(\mathbf{u}) + \\ &\quad \int_{\mathbb{R}^m} k_Z((\mathbf{x}, \mathbf{u}); \mathcal{X}_n \times \mathcal{U}_n) k_Z(\mathcal{X}_n \times \mathcal{U}_n; \mathcal{X}_n \times \mathcal{U}_n)^{-1} (\mathbf{Z} - m_Z(\mathcal{X}_n \times \mathcal{U}_n)) d\rho(\mathbf{u}), \end{aligned} \quad (8)$$

and

$$\begin{aligned} \text{Cov}(Y_{\mathbf{x}}^n, Y_{\mathbf{x}'}^n) &= \int_{\mathbb{R}^m} \int_{\mathbb{R}^m} k_Z((\mathbf{x}, \mathbf{u}); (\mathbf{x}', \mathbf{u}')) \\ &\quad - k_Z((\mathbf{x}, \mathbf{u}); \mathcal{X}_n \times \mathcal{U}_n) k_Z(\mathcal{X}_n \times \mathcal{U}_n; \mathcal{X}_n \times \mathcal{U}_n)^{-1} k_Z(\mathcal{X}_n \times \mathcal{U}_n; (\mathbf{x}', \mathbf{u}')) d\rho(\mathbf{u}) d\rho(\mathbf{u}'). \end{aligned} \quad (9)$$

3. Data driven infill strategy for stochastic inversion

In this section we propose a two-step infill strategy in the joint space. The first step consists in choosing a point in the control space while the second one aims at enriching the design with a new point in the uncertain space.

3.1. Minimization of the Vorob'ev deviation: choice of next \mathbf{x}

The objective of the first step is to wisely choose the points in the control space \mathbb{X} in order to accurately estimate the set $\Gamma^* = \{\mathbf{x} \in \mathbb{X}, g(\mathbf{x}) = \mathbb{E}_{\mathbf{V}}[f(\mathbf{x}, \mathbf{V})] \leq c\}$. For this purpose, we consider the statistical model of the non-observable function g given by $Y_{\mathbf{x}}^n$ introduced in Section 2.3. Due to the stochastic nature of $(Y_{\mathbf{x}}^n)_{\mathbf{x} \in \mathbb{X}}$, the associated excursion set,

$$\Gamma = \{\mathbf{x} \in \mathbb{X}, Y_{\mathbf{x}}^n \leq c\} \quad (10)$$

is a well defined random closed set if $(Y_{\mathbf{x}}^n)_{\mathbf{x} \in \mathbb{X}}$ has continuous sample paths ([Mol06] p.4, 23). Therefore, from now on, the considered random processes will be supposed separable ([Doo53], p.57), the mean m_Z to be continuous and the covariance function k_Z to be Matérn (5/2 or 3/2). Indeed, under these assumptions, we know that $(Z_{(\mathbf{x}, \mathbf{u})})_{(\mathbf{x}, \mathbf{u}) \in \mathbb{X} \times \mathbb{R}^m}$ has continuous sample paths ([Pac03] p.44 table 2.1) and we can prove that the path continuity property remains valid for the integrated conditioned process $(Y_{\mathbf{x}}^n)_{\mathbf{x} \in \mathbb{X}}$ by using the necessary criterion introduced in [Adl81] p.60 and presented in [Pac03] p.38 Eq.(2.9).

From the assumption that g is a realization of $Y_{\mathbf{x}}^n$, the true unknown set Γ^* can be seen as a realization of the random closed set Γ . The book of [Mol06] gives many possible definitions for the variance of a random closed set. In the present work we adapt the Stepwise Uncertainty Reduction (SUR) strategy introduced in [CG13] which aims at decreasing an uncertainty function defined as the Vorob'ev deviation ([Vor84, VL13]) of the random set.

More precisely the uncertainty function at step n is defined as

$$\mathcal{H}_n^{\text{uncert}} = \mathbb{E}[\mu(\Gamma \Delta Q_{n, \alpha_n^*}) \mid Z_{\mathcal{X}_n \times \mathcal{U}_n} = \mathbf{Z}_n],$$

where μ is the Lebesgue measure on \mathbb{X} , Δ the symmetric difference operator between two sets, the Vorob'ev quantiles are given by $Q_{n, \alpha} = \{\mathbf{x} \in \mathbb{X}, \mathbb{P}(Y_{\mathbf{x}}^n \leq c) \geq \alpha\}$, and the Vorob'ev expectation Q_{n, α_n^*} can be determined by tuning α to a level α^* such that $\mu(Q_{n, \alpha_n^*}) = \mathbb{E}[\mu(\Gamma) \mid Z_{\mathcal{X}_n \times \mathcal{U}_n} = \mathbf{Z}_n]$. Let

$$\mathcal{H}_{n+1}^{\text{uncert}}(\mathbf{x}) = \mathbb{E}[\mu(\Gamma \Delta Q_{n+1, \alpha_{n+1}^*}) \mid Z_{\mathcal{X}_n \times \mathcal{U}_n} = \mathbf{Z}_n, Y_{\mathbf{x}}^n].$$

The objective of the SUR strategy is thus to enrich the current design with a new point \mathbf{x}_{n+1} satisfying

$$\begin{aligned} \mathbf{x}_{n+1} &\in \operatorname{argmin}_{\mathbf{x} \in \mathbb{X}} \mathbb{E}_{n, \mathbf{x}}[\mathcal{H}_{n+1}^{\text{uncert}}(\mathbf{x})] \\ &:= \operatorname{argmin}_{\mathbf{x} \in \mathbb{X}} \mathcal{J}_n(\mathbf{x}), \end{aligned} \quad (11)$$

where $\mathbb{E}_{n, \mathbf{x}}$ denotes the expectation with respect to $Y_{\mathbf{x}}^n$ (for detailed formula and estimation of $\mathcal{J}_n(\cdot)$ see [CG13]).

The enrichment of the DoE consists in selecting a couple $(\mathbf{x}_{n+1}, \mathbf{u}_{n+1})$ in the joint space $\mathbb{X} \times \mathbb{R}^m$. \mathbf{x}_{n+1} has just been defined by (11), it remains now to choose a new point u_{n+1} in the uncertain space.

3.2. Minimization of the variance: choice of next \mathbf{u}

The process Y^n approximates the expectation $\mathbb{E}_{\mathbf{V}}[f(\cdot, \mathbf{V})]$. It can be seen as a projection of Z^n from the joint space onto the control space. We propose to sample the point \mathbf{u}_{n+1} in the uncertain space in order to reduce at most the one-step-ahead variance at point \mathbf{x}_{n+1} , $\text{VAR}(Y_{\mathbf{x}_{n+1}}^{n+1})$, whose expression is obtained from Eq.(9). More precisely,

$$\mathbf{u}_{n+1} = \underset{\tilde{\mathbf{u}} \in \mathbb{R}^m}{\text{argmin}} \text{VAR}(Y_{\mathbf{x}_{n+1}}^{n+1}), \quad (12)$$

with

$$\begin{aligned} \text{VAR}(Y_{\mathbf{x}_{n+1}}^{n+1}) &= \vartheta(\tilde{\mathbf{u}}) \\ &= \int_{\mathbb{R}^m} \int_{\mathbb{R}^m} k_Z((\mathbf{x}_{n+1}, \mathbf{u}); (\mathbf{x}_{n+1}, \mathbf{u}')) d\rho(\mathbf{u}) d\rho(\mathbf{u}') \\ &\quad - \int_{\mathbb{R}^m} \int_{\mathbb{R}^m} k_Z((\mathbf{x}_{n+1}, \mathbf{u}); \mathcal{X}_{n+1} \times \mathcal{U}_{n+1}) \\ &\quad k_Z(\mathcal{X}_{n+1} \times \mathcal{U}_{n+1}; \mathcal{X}_{n+1} \times \mathcal{U}_{n+1})^{-1} k_Z(\mathcal{X}_{n+1} \times \mathcal{U}_{n+1}; (\mathbf{x}_{n+1}, \mathbf{u}')) d\rho(\mathbf{u}) d\rho(\mathbf{u}'), \end{aligned} \quad (13)$$

where $\mathcal{X}_{n+1} \times \mathcal{U}_{n+1} = \mathcal{X}_n \times \mathcal{U}_n \cup \{(\mathbf{x}_{n+1}, \tilde{\mathbf{u}})\}$.

3.3. Implementation

The setting of our procedure is driven by our industrial application where the probability distribution of the uncertain variable V is known only through a finite set of realizations $\Xi = \{\check{\mathbf{v}}_1, \dots, \check{\mathbf{v}}_N\}$.

Computational method for functional PCA. We consider the empirical version of $C(s, t)$ defined

as $C^N(s, t) = \frac{1}{N} \sum_{i=1}^N \check{\mathbf{v}}_i(s) \check{\mathbf{v}}_i(t)$. The eigenvalue problem defined by Eq. (3) is then solved by

discretizing the trajectories $\{\check{\mathbf{v}}_i\}_{i=1, \dots, N}$ on $[0, T]$ and replacing C by C^N .

Denoting by $\hat{\psi}_i$, $i = 1, \dots, m$, the m first estimated eigenfunctions, we define

$$\mathcal{G}_m = \{\check{\mathbf{u}}_1, \dots, \check{\mathbf{u}}_m\} \quad (14)$$

with $\check{\mathbf{u}}_i = (\langle \check{\mathbf{v}}_i, \hat{\psi}_1 \rangle, \dots, \langle \check{\mathbf{v}}_i, \hat{\psi}_m \rangle)^T$.

Minimization of the one-step-ahead variance. Since \mathbf{V} is known through a finite set Ξ , Eq. (12) is solved on the finite set \mathcal{G}_m .

We now detail the implementation of our methodology. Let us first state the global algorithm and then comment some of its steps.

Algorithm 1 Stochastic inversion via joint space modelling

Require: The truncation argument m , the DoE of n_0 points $\mathcal{X}_{n_0} \times \mathcal{U}_{n_0}$ in $\mathbb{X} \times \mathcal{G}_m$ and a maximal simulation budget

- 1: Set $n = n_0$.
 - 2: Calculate \mathbf{Z} the simulator responses at the design points $\mathcal{X}_n \times \mathcal{U}_n$
 - 3: **while** $n \leq \text{budget}$ **do**
 - 4: Fit the GP model Z^n
 - 5: Induce the integrated GP $Y_{\mathbf{x}}^n$
 - 6: $\mathbf{x}_{n+1} \leftarrow$ sampling criterion \mathcal{J}_n
 - 7: $\mathbf{u}_{n+1} \leftarrow \operatorname{argmin}_{\bar{\mathbf{u}} \in \mathcal{G}_m} \mathbb{V}\mathbb{A}\mathbb{R}(Y_{\mathbf{x}_{n+1}}^{n+1})$
 - 8: Simulation at $(\mathbf{x}_{n+1}, \mathbf{v}_{n+1})$, where $\mathbf{v}_{n+1} \in \Xi$ is the curve corresponding to \mathbf{u}_{n+1}
 - 9: Update DoE : $\mathcal{X}_{n+1} \times \mathcal{U}_{n+1} = \mathcal{X}_n \times \mathcal{U}_n \cup \{(\mathbf{x}_{n+1}, \mathbf{v}_{n+1})\}$
 - 10: Update $\mathbf{Z} = \mathbf{Z} \cup \{f(\mathbf{x}_{n+1}, \mathbf{v}_{n+1})\}$
 - 11: Set $n = n + 1$
 - 12: **end while**
 - 13: Fit the final GP model Z^n
 - 14: Approximate Γ^* by the Vorob'ev expectation
-

- step 1** Let \mathbb{U} be the smallest m -rectangle containing \mathcal{G}_m , $\mathbb{U} = \prod_{i=1}^m [\min(\langle \Xi, \hat{\psi}_i \rangle), \max(\langle \Xi, \hat{\psi}_i \rangle)]$. For the initial DoE, we first build a Random Latin Hypercube Design of n points $\mathcal{X}_n \times \bar{\mathcal{U}}_n$ in the joint space (\mathbb{X}, \mathbb{U}) . Then the set of points \mathcal{U}_n is determined such that for $i = 1, \dots, n$, $\mathbf{u}_i \in \mathcal{G}_m$ is the closest point from $\bar{\mathbf{u}}_i \in \bar{\mathcal{U}}_n$ (with respect to the euclidean norm in \mathbb{R}^m).
- step 4** The covariance kernel of the GP is chosen as a Matérn-5/2 covariance and we add a noise modelled with a constant variance term. The homoscedastic modelling of the noise is discussed in Section 4.3. The mean function of the GP is modelled by a constant function. All types of parameters (mean, correlation lengths, variance and noise) are estimated by maximum likelihood [RGD12].
- step 5** In the framework where the uncertain vector \mathbf{U} is Gaussian as well as the covariance kernel, closed form solutions of the integrals in (8) and (9) are given in [JLR13]. In our framework, the integrals in (8) and (9) are approximated by Monte Carlo.
- step 6** \mathbf{x}_{n+1} is obtained by solving (11) with a continuous global optimization algorithm: GENetic Optimization Using Derivatives (GENOUD) [JS11].
- step 7** Once more the integrals in (13) are approximated by Monte Carlo. More details on the estimation of (13) can be found in [JLR13]. Here the minimization problem is solved by an exhaustive search on the finite set \mathcal{G}_m defined in (14).
- step 8** The simulator is evaluated at point $(\mathbf{x}_{n+1}, \mathbf{v}_{n+1})$ where \mathbf{v}_{n+1} is the curve of the initial set of curves Ξ corresponding to the truncated vector of coefficients \mathbf{u}_{n+1} . Note that evaluating the simulator at a curve in the initial set of realizations whose coordinate in the uncertain space is \mathbf{u}_{n+1} and not a projected curve on the basis composed with first eigenfunctions brings robustness with respect to the truncation argument.

4. Numerical experiments

4.1. Two analytical examples - set-up

To illustrate the behaviour of the proposed algorithm 1, we consider two analytical examples. We suppose that a sample Ξ of $N = 200$ realizations of the functional random variable \mathbf{V} is available and its probability distribution is unknown. To highlight the robustness of our method regarding

the random distribution of the uncertainties, we consider two types of functional random variables: Brownian motion and max-stable process. As Algorithm 1 depends on the truncation argument m , different values are tested (see Table.4.1) to better understand the effect of the uncertain space dimension.

m	2	4	8
\mathbf{V} : Brownian motion	90.1 %	95.2 %	97.6%
\mathbf{V} : Max-stable process	58.8 %	63.3 %	70%

Table 1: The explained variance of the functional data by the reduced variables in function of m for two types of uncertainties.

For the next two analytical examples, we consider a Gaussian Process prior $Z_{(\mathbf{x}, \mathbf{u})}$ with constant mean and Matèrn covariance kernel with $\nu = 5/2$. Random Latin Hypercube Designs (RLHD) are used as initial DoEs in all the experiments . The number of points of the initial DoE is 20 for the first analytical example and 30 for the second one. RLHD induce variability in the behaviour of the algorithms. To account for this variability, the performance of each method is averaged over 30 (respectively 10) independent runs for Brownian motion (respectively max-stable process).

Analytical example 1. We consider an additive function, sum of the two-dimensional Bo-hachevsky function and a random term, defined as

$$f : (\mathbf{x}, \mathbf{V}) \mapsto (x_1^2 + 2x_2^2 - 0.3 \cos(3\pi x_1) - 0.4 \cos(4\pi x_2) + 0.7) + \int_0^T e^{\mathbf{V}t} dt,$$

where $\mathbf{x} \in \mathbb{X} = [-100, 100]^2$. The objective is to approximate the set $\Gamma^* = \{\mathbf{x} \in \mathbb{X}, g(\mathbf{x}) = \mathbb{E}_{\mathbf{V}}[f(\mathbf{x}, \mathbf{V})] \leq 3500\}$ for the two different types of distribution of the random functional variable (Brownian motion and max-stable process).

Analytical example 2. For the second example we define a function that is not separable with respect to the control variables and uncertainties. The function involves the maximum and the minimum of $(V_t)_{t \geq 0}$, so catching the whole variability of \mathbf{V} becomes important. The function f is given by

$$f : (\mathbf{x}, \mathbf{V}) \mapsto \max_t \mathbf{V}_t |0.1 \cos(x_1 \max_t \mathbf{V}_t) \sin(x_2)(x_1 + x_2 \min_t \mathbf{V}_t)^2| \int_0^T (30 + \mathbf{V}_t)^{\frac{x_1 x_2}{20}} dt,$$

where the control variables lie in $\mathbb{X} = [1.5, 5] \times [3.5, 5]$. The objective is to approximate the set $\Gamma^* = \{\mathbf{x} \in \mathbb{X}, g(\mathbf{x}) = \mathbb{E}_{\mathbf{V}}[f(\mathbf{x}, \mathbf{V})] \leq c\}$, when $c = 1.2$ and $c = 0.9$ for the Brownian motion and the max-stable Process respectively.

To compare the performance of both algorithms, we use the ratio of the volume of the symmetric difference between the true set Γ^* and the estimated set Q_{n, α^*} : $\mu(\Gamma^* \Delta Q_{n, \alpha^*}) / \mu(\Gamma^*)$ to which we will refer by the quality-ratio.

4.2. Two analytical examples - results

In Figures 1 and 2, we show the evolution of the averaged quality-ratio with respect to the number of simulations involved in the Algorithm 1 on the two analytical examples with the two types of functional uncertainties (Brownian and max-stable process). The average is taken over

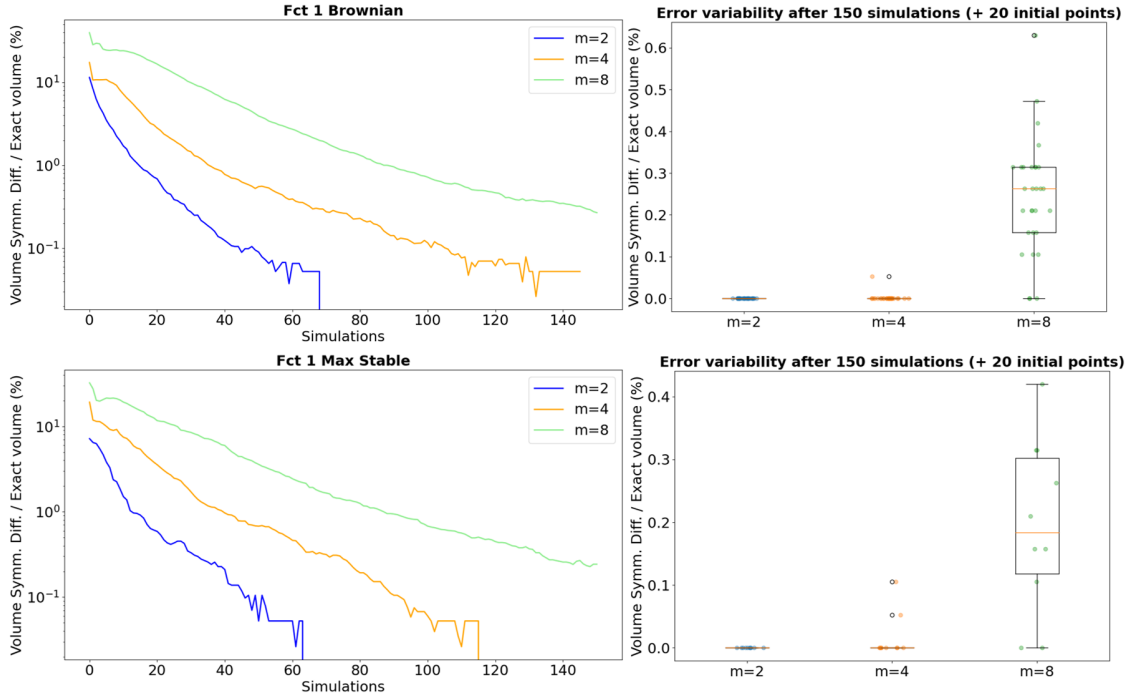


Figure 1: Analytical example 1 with Brownian motion (top) and with max-stable process (bottom). Convergence of Algorithm 1 for $m = \{2, 4, 8\}$. Left: mean of the symmetric differences vs. number of simulator calls in log scale. The mean is taken over the independent runs of initial RLHD. Right: symmetric differences associated with the random initial DoEs at the maximal simulation budget.

the repeated runs of the complete approach corresponding to the 30 random initial designs (10 for the max-table process), and for 3 values of the truncation argument m .

For the first analytical example, the smaller values of m , the faster is the convergence. This observation can be explained by the fact that, in higher dimensional joined space (due to larger values of m), much more evaluation points are necessary to learn an accurate GP model (more hyper-parameters to determine). It is worth noting that even for 90% (for Brownian motion) or 58.8% (for max-stable process) of explained variance with $m = 2$ the proposed algorithm provides an efficient estimate of the true set Γ^* . Indeed, on stage 8 in Algorithm 1 the full curve $\mathbf{v}_{n+1} \in \Xi$ associated to \mathbf{u}_{n+1} is recovered, such that the information lost after the dimension reduction is reduced, thereby further robustifying the method.

For the second analytical example, the output depends on local behaviours of the stochastic process. The truncation argument $m = 2$ is too small to catch these dependencies, the function is sensitive to higher KL order. For the Brownian motion, more than 95% of variance is explained with $m = 4$. It seems sufficient to obtain an accurate approximation of Γ^* . The improvement between $m = 2$ and $m = 4$ is noticeable. The improvement is not as important when the uncertainties are driven by a max-stable process since the percentage of explained variance increases slowly. Better results should be observed with $m = 8$. It is not the case because a higher dimension leads to difficulties in the estimation of the GP except by increasing consequently the number of observation points.

In Figure 3 we can see the evolution of the feasible domain estimation with respect to the iterations of Algorithm 1 for the second analytic case and the Brownian motion, and for different truncation levels. From left to right we observe the increase of additional sampling points near the

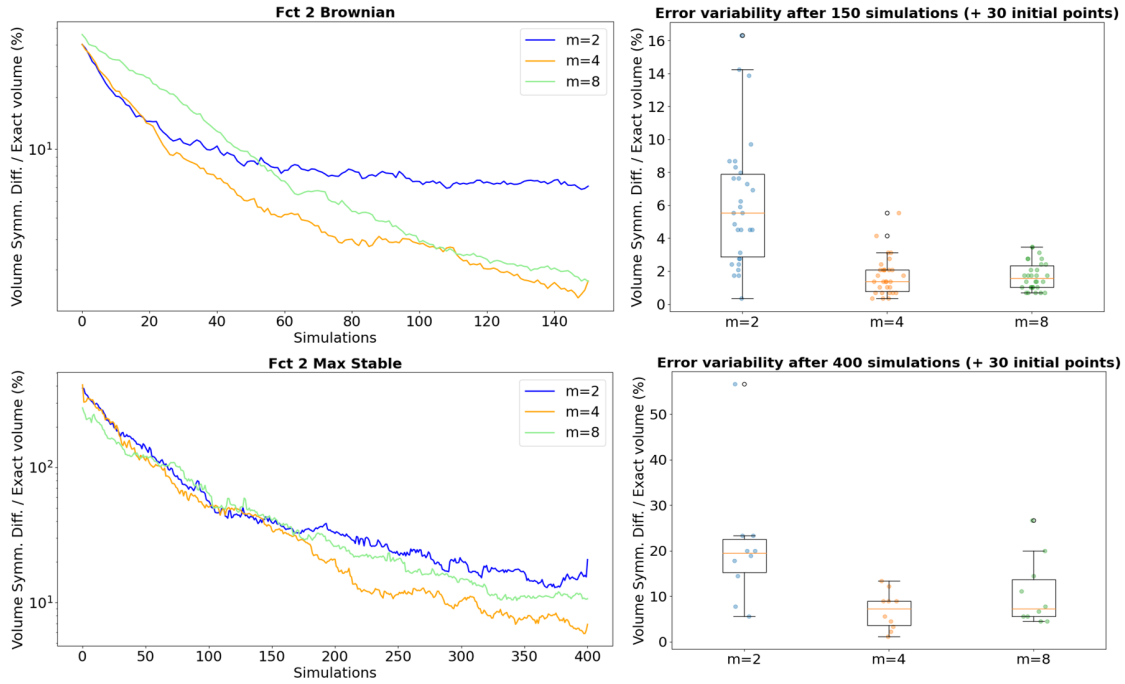


Figure 2: Analytical example 2 with Brownian motion (top) and with max-stable process (bottom). Convergence of Algorithm 1 for $m = \{2, 4, 8\}$. Left: mean of the symmetric differences vs. number of simulator calls in log scale. The mean is taken over the independent runs of initial RLHD. Right: symmetric differences associated with the random initial DoEs at the maximal simulation budget.

boundary with the iteration number.

As shown in Figure 4, the larger the dimension of the problem is, the larger the computational cost is. Moreover, the computational time needed to provide the next evaluation point increases with the number of simulator calls, and thus with the number of iterations, because of the cost of Kriging approximation directly linked with the learning sample size. For example in the case of $m = 8$ (resp. $m = 2$), iteration 80 requires 203 (resp. 126) seconds to provide the next evaluation point whereas iteration 150 requires 275 (resp. 164) seconds.

In this section, we also compare the sampling criterion in the uncertain space, based on (11), with a uniform sampling. Among the experiments we conducted, we show the results obtained for the analytical case 1 and the Brownian motion. The points selected with the criterion based on (11) seems to concentrate on interest zones, in comparison to the points selected uniformly (see Figures 5 and 6).

It is also interesting to compare the evolution of the estimation error, defined as the relative symmetric difference volume. We see on Figures 7 and 8 that the criterion based on (11) leads to a faster decrease of the relative symmetric difference volume and to a much smaller error variability, in comparison to a uniform sampling in the uncertain space.

To conclude the analysis of stochastic inversion on both analytical cases, we compare the method proposed in this paper, based on joint metamodeling, with the approach introduced in [EAHL⁺20] which combines metamodeling in the control space with quantization for the estimation of the expectation in the uncertain space. Even without compatibilizing the costs induced by the initial designs (RLHD of size 9), the current approach based on joint metamodeling performs better regardless of the truncation argument m (Figure 9). Adding the costs induced by the quantization on the initial sample points would disadvantage even more the approach introduced in [EAHL⁺20]

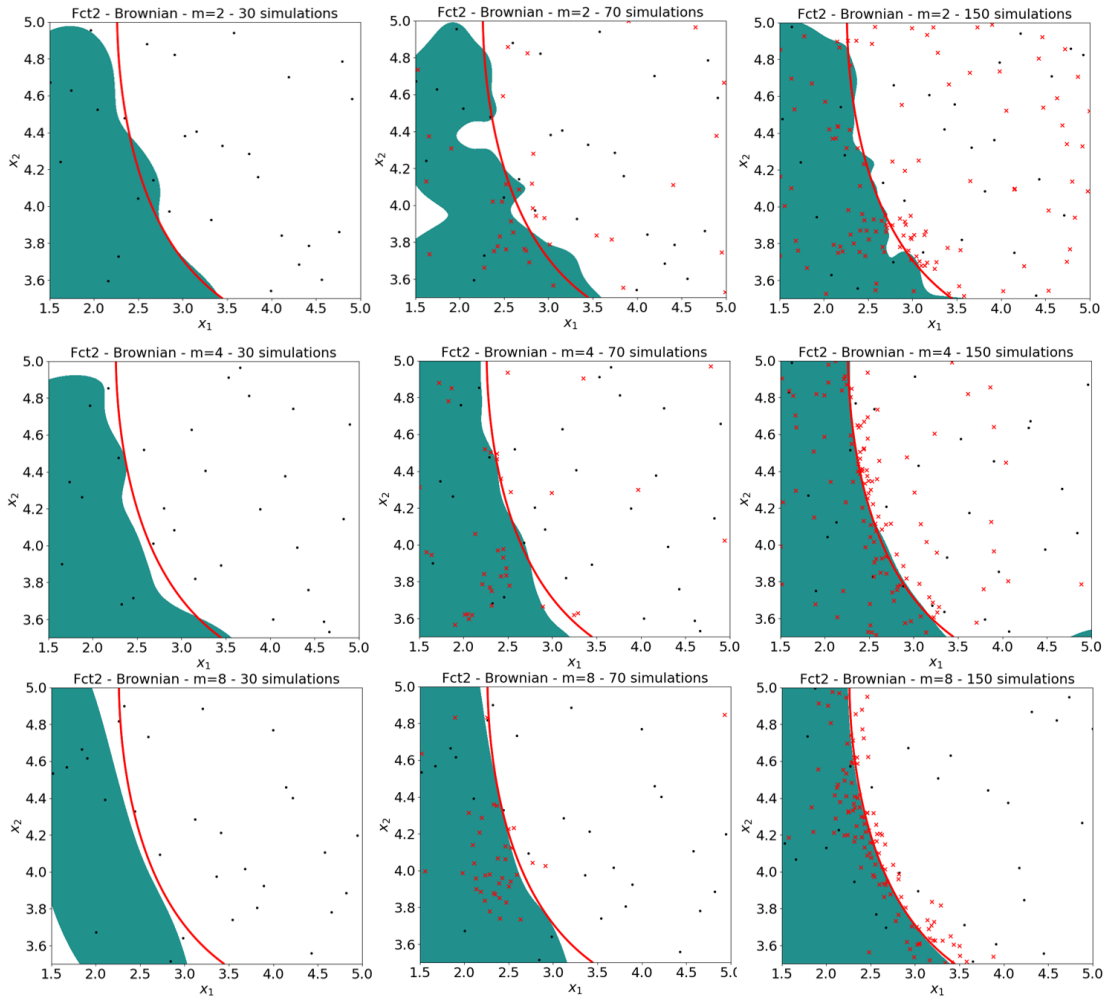


Figure 3: Feasible domain estimation for function 2 with Brownian motion in green and its boundary in red for 3 different iterations (30, 70 and 150 from left to right) and for the 3 values of $m = 2, 4$ and 8 (from top to bottom). The black dots are the \mathbf{x} coordinates of the points in the initial design of experiments, the red crosses are the additional points chosen by the algorithm.

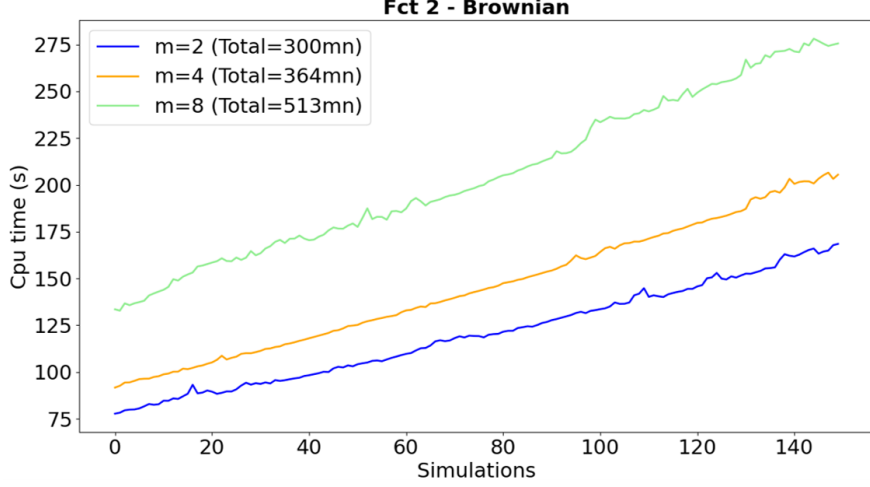


Figure 4: The computational time (sec.) needed to provide the next evaluation point as a function of iterations for the second analytic example with Brownian motion. The values are averaged computational times for 5 runs of each strategy: $m = 2, 4, 8$.

as the averaged size of the quantizer is around 20 for each of the points (in the control space) of the initial design. It means that for each point of the initial design (RLHD with 9 points in the control space), the expectation is estimated by evaluating the model on the quantizer (in the uncertain space), that is by evaluating the model on 20 points (in the joint space) if the quantizer is of size 20.

4.3. Discussion on the GP model on the finite-dimensional truncated space

We discuss here the assumption stated in Section 2.2 that $f(\mathbf{x}, \mathbf{v})$ is a realization of a Gaussian Process $Z_{(\mathbf{x}, \mathbf{u})}$ defined on the truncated space $\mathbb{X} \times \mathbb{R}^m$. It is worth underlying here that our aim was to reduce the simulation cost by considering a m -truncation of the KL expansion while accounting for our partial knowledge on the distribution of \mathbf{V} through only a finite sample of realizations. Let us consider two truncation arguments m and $L > m$, with L large enough to ensure that the part of variance explained by the KL terms indexed by $i > L$ is negligible. For a given realization \mathbf{v} of \mathbf{V} , let us introduce the notation $(\mathbf{u}, \tilde{\mathbf{u}}) \in \mathbb{R}^m \times \mathbb{R}^{L-m}$ where $\mathbf{u} = (\langle \mathbf{v}, \hat{\psi}_1 \rangle, \dots, \langle \mathbf{v}, \hat{\psi}_m \rangle)^\top$ and $\tilde{\mathbf{u}} = (\langle \mathbf{v}, \hat{\psi}_{m+1} \rangle, \dots, \langle \mathbf{v}, \hat{\psi}_L \rangle)^\top$. In that setting $f(\mathbf{x}, \mathbf{V})$ can be expressed as

$$f(\mathbf{x}, \mathbf{V}) = f(\mathbf{x}, \hat{\mathbf{V}}_L) + \epsilon_T = f(\mathbf{x}, (\mathbf{U}, \tilde{\mathbf{U}})\hat{\Phi}_L) + \epsilon_T$$

where $\hat{\mathbf{V}}_L$ is the empirical version (estimated from C^N) of the KL approximation of \mathbf{V} given by (4) (replacing m by L), $\hat{\Phi}_L = (\hat{\psi}_1, \dots, \hat{\psi}_L)^\top$ and ϵ_T is the error associated to the KL truncation and empirical approximation, supposed small by construction.

Then, the best L^2 -approximation of $f(\mathbf{x}, (\mathbf{U}, \tilde{\mathbf{U}})\hat{\Phi}_L)$ by a measurable function of \mathbf{U} only is the conditional expectation $\mathbb{E}_{\tilde{\mathbf{U}}} [f(\mathbf{x}, (\mathbf{U}, \tilde{\mathbf{U}})\hat{\Phi}_L) | \mathbf{U}]$. We thus write:

$$f(\mathbf{x}, \mathbf{V}) = \mathbb{E}_{\tilde{\mathbf{U}}} [f(\mathbf{x}, (\mathbf{U}, \tilde{\mathbf{U}})\hat{\Phi}_L) | \mathbf{U}] + \epsilon_P + \epsilon_T$$

with ϵ_P the L^2 -projection error. We can further approximate the conditional expectation by

$$f(\mathbf{x}, (\mathbf{U}, \tilde{\mathbf{u}}(\mathbf{U}))\hat{\Phi}_L) + \epsilon_E$$

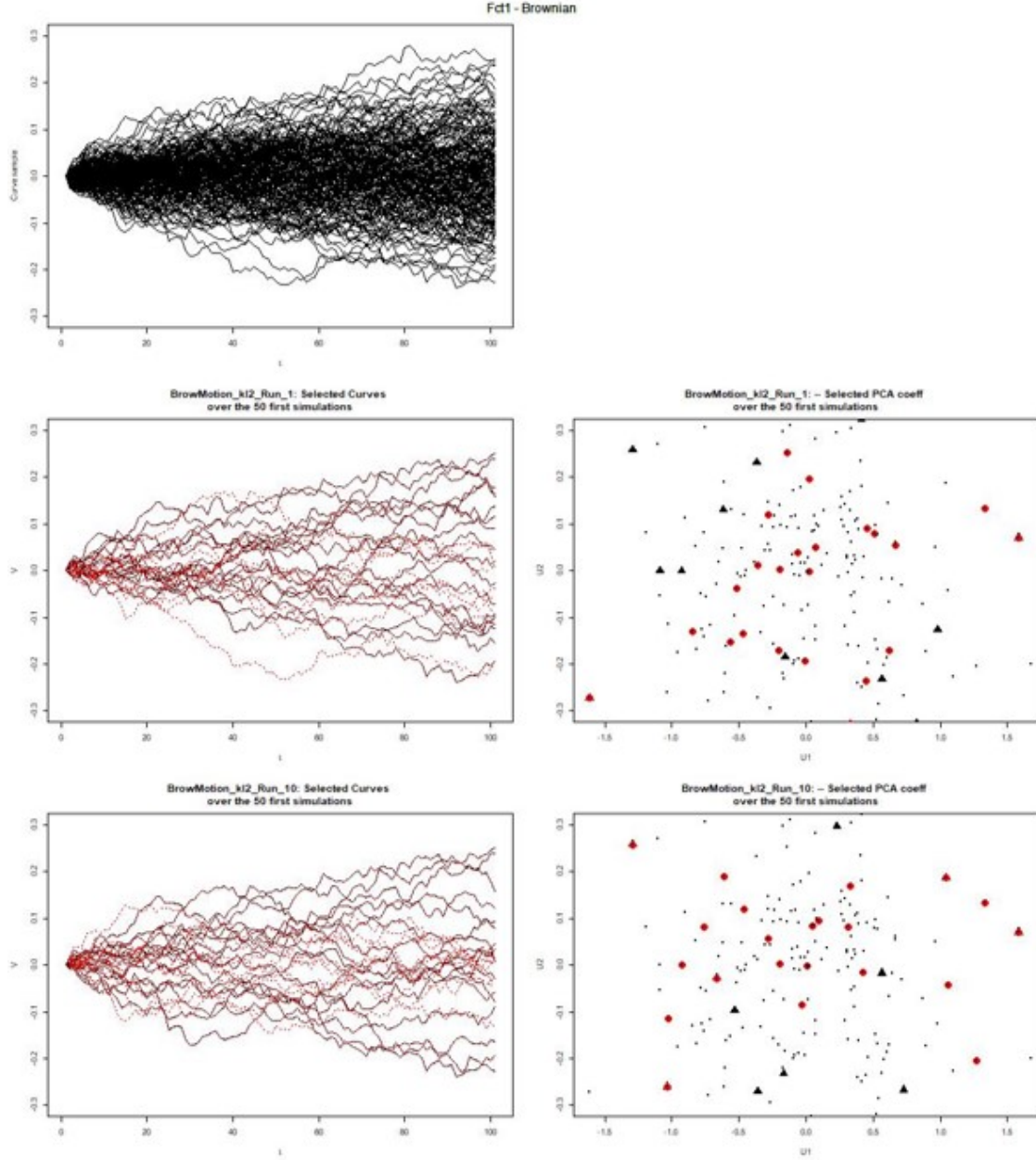


Figure 5: Analytical case 1 with the uncertainty modelled by a Brownian motion. (right) Black triangles correspond to the coefficients of the initial RLHD plotted in the uncertain truncated space. Red points are added points uniformly sampled up to 50 simulations. (left) The corresponding selected curves among the whole set of realizations (displayed at top).

where $\tilde{\mathbf{u}}(\mathbf{U})$ is one realization of $\tilde{\mathbf{U}}|\mathbf{U}$ and ϵ_E accounts for the expectation approximation. The latter approximation is motivated by the fact that, since \mathbf{V} is only known through a finite sample, we only have access to one $\tilde{\mathbf{u}}(\mathbf{u})$ realization for each \mathbf{u} corresponding to \mathbf{v} in the initial finite set Ξ . Thus we can write:

$$f(\mathbf{x}, \mathbf{V}) = f(\mathbf{x}, (\mathbf{U}, \tilde{\mathbf{u}}(\mathbf{U}))\hat{\Phi}_L) + \epsilon \quad (15)$$

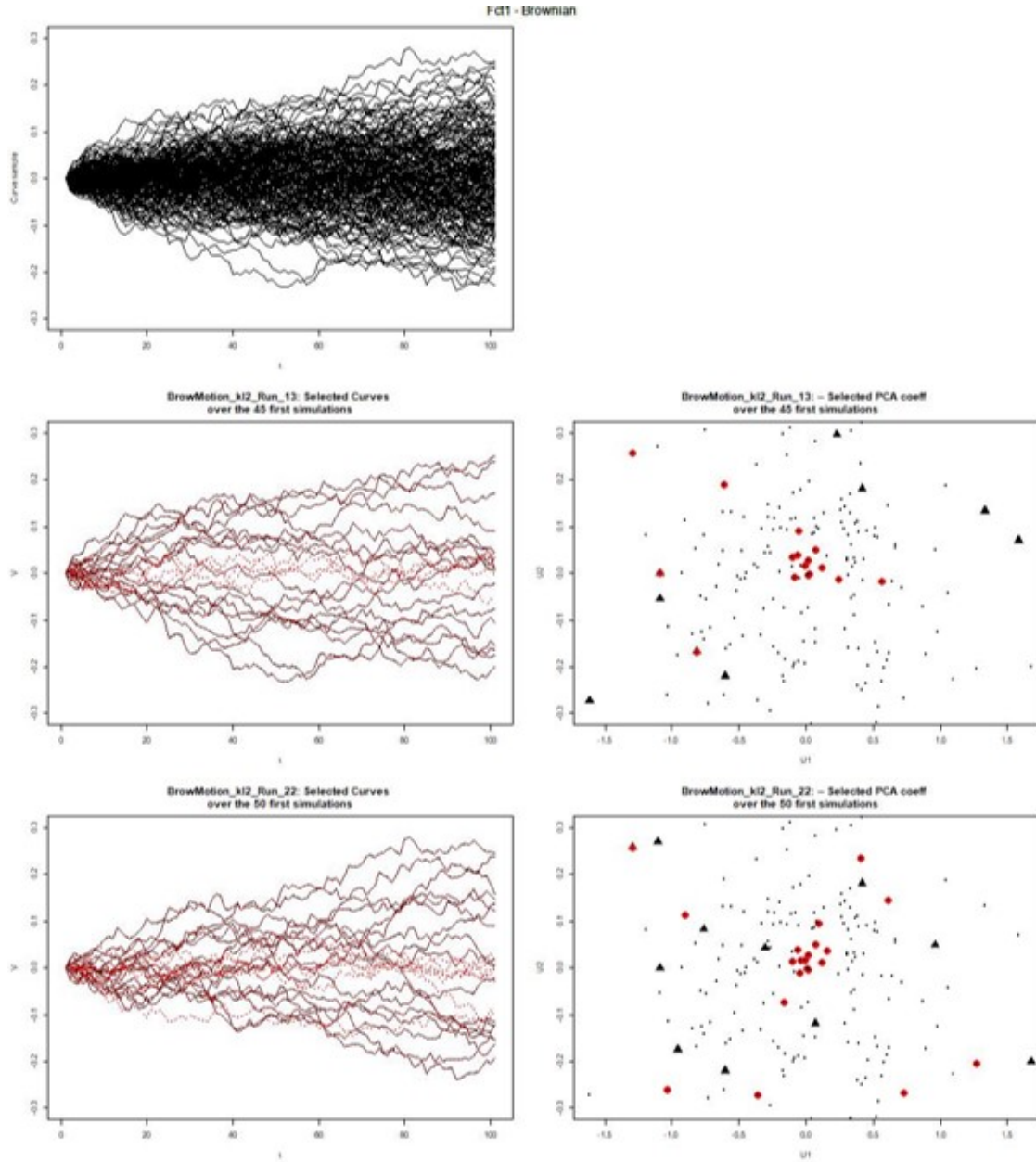


Figure 6: Analytical case 1 with the uncertainty modelled by a Brownian motion. (right) Black triangles correspond to the coefficients of the initial RLHD plotted in the uncertain truncated space. Red points are selected with our criterion up to 50 simulations. (left) The corresponding selected curves among the whole set of realizations (displayed at top).

with $\epsilon = \epsilon_T + \epsilon_P + \epsilon_E$. According to this last equation, the modelling assumption in Section 2.2 should include a noise term. However, the estimation of this heteroscedastic noise comes with an extra estimation cost and as it can be seen in Figure 10, no significant model improvement is observed. Indeed in Figure 10, for $m = 2$, we present the evolution of the symmetric difference for the noisy GP model $Z_{(\mathbf{x}, \mathbf{u})}$ introduced from equation (15) when the noise ϵ is Gaussian and

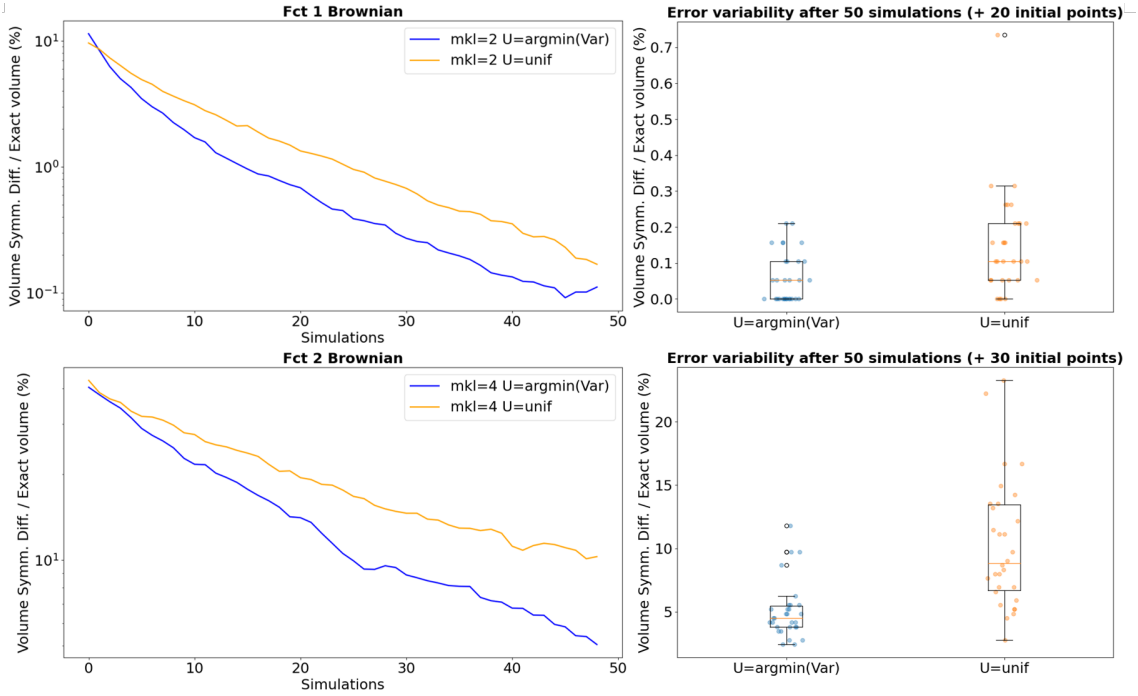


Figure 7: Decrease of the relative symmetric difference volume (left) and boxplots for the errors (right) for the first analytical case (top) and the second one (bottom) for the Brownian motion, comparing criterion based on (11) with the uniform sampling in the uncertain space.

heteroscedastic with a variance function of (\mathbf{x}, \mathbf{u}) :

$$\tau^2(\mathbf{x}, \mathbf{u}) = \text{Var}_{\tilde{\mathbf{U}}} [f(\mathbf{x}, (\mathbf{u}, \tilde{\mathbf{U}}(\mathbf{u})) \hat{\Phi}_L) | \mathbf{U} = \mathbf{u}].$$

Moreover, supposing \mathbf{V} Gaussian or "nearly Gaussian", that is assuming that $\tilde{\mathbf{U}}$ can be considered in first approximation as independent of \mathbf{U} , then $\tau^2(\mathbf{x}, \mathbf{u})$ can be estimated by

$$\hat{\tau}^2(\mathbf{x}, \mathbf{u}) = \sum_{k=1}^l w_k [f(\mathbf{x}, \mathbf{V}_k^{Quant}) - \sum_{j=1}^l w_j f(\mathbf{x}, \mathbf{V}_j^{Quant})]^2$$

where $l = 5$ and the \mathbf{V}_k^{Quant} are greedy functional quantizers and w_k associated weights (see [EAHL⁺20] for more details). These quantizers are built from a set of N curves $\{(\mathbf{u}, \tilde{\mathbf{u}}_k) \hat{\Phi}_L, k = 1, \dots, N\}$ where $\tilde{\mathbf{u}}_k$ are independent samples of $\tilde{\mathbf{U}}$ which in practice are uniformly sampled in the finite set $\tilde{\mathcal{G}}_{m,L} = \{\tilde{\mathbf{u}}_1, \dots, \tilde{\mathbf{u}}_N\}$ where $\tilde{\mathbf{u}}_i = (\langle \check{v}_i, \hat{\psi}_{m+1} \rangle, \dots, \langle \check{v}_i, \hat{\psi}_L \rangle)$. Numerically we select 20 (\mathbf{x}, \mathbf{u}) -points from the initial DoE set of size $n = 30$ and estimate the corresponding $\hat{\tau}^2$. To avoid further estimation of τ^2 at new locations (the remaining DoE points and during the infill strategy), we build a second GP model of $\log(\hat{\tau}^2)$ based on the 20 initial estimations. Finally the noisy GP model Z is built using as noise variance $\exp(\hat{\log}(\hat{\tau}^2))$. Overall we need additional $l \times 20 = 100$ costly evaluations of f to estimate the heteroscedastic noise.

In Figure 10 we notice that compared to the homoscedastic model with $m = 2$, the model with heteroscedastic noise achieves a faster symmetric difference volume reduction but the overcost, for the variance estimation, makes this approach interesting only for a large simulation budget: at least 130 simulations. For the Brownian case, on function 2, the homoscedastic models with higher m still perform better for a budget up to 150 than the heteroscedastic one. A model with a small

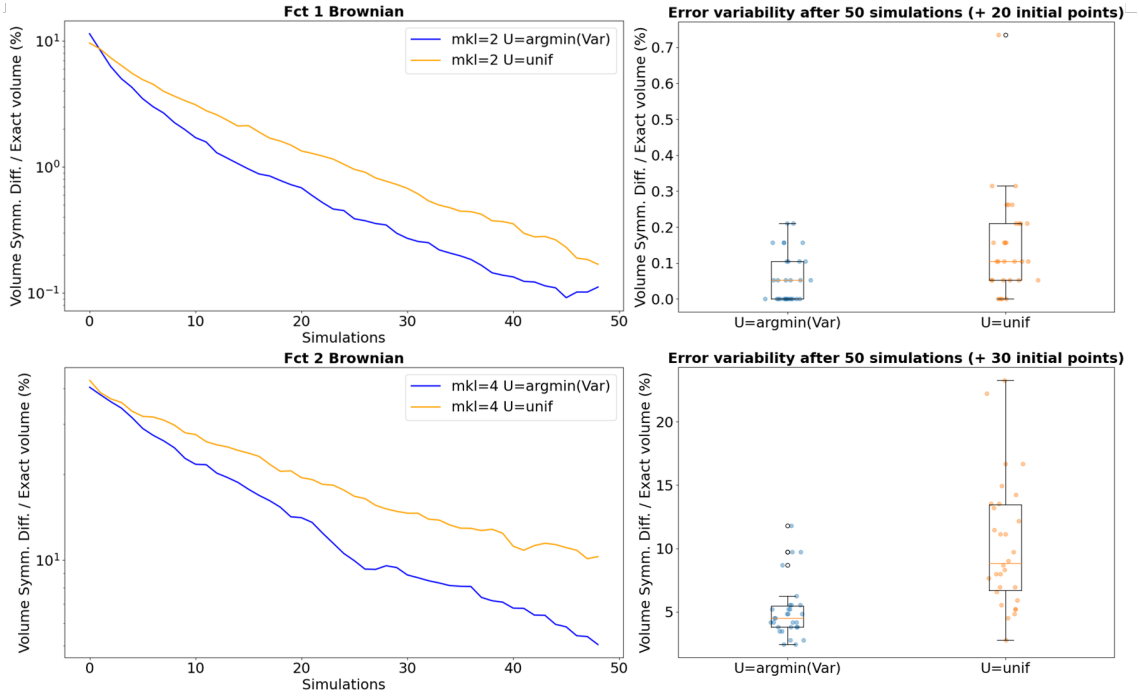


Figure 8: Decrease of the relative symmetric difference volume (left) and boxplots for the errors (right) for the first analytical case (top) and the second one (bottom) for the Max Stable process, comparing criterion based on (11) with the uniform sampling in the uncertain space.

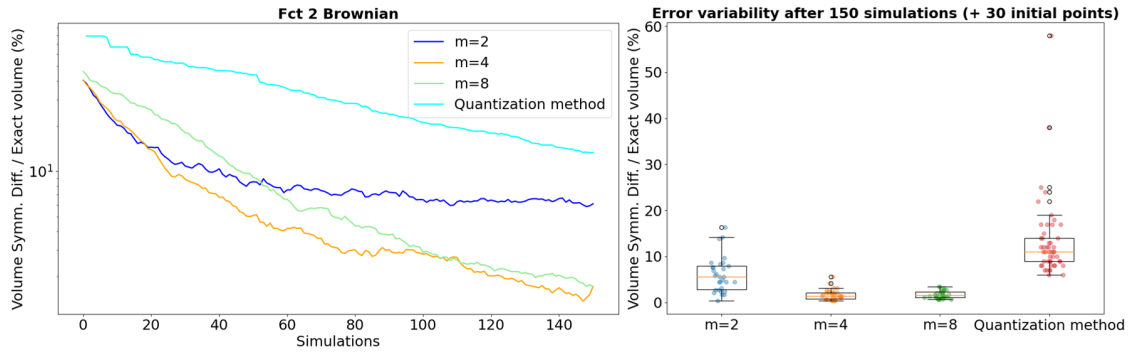


Figure 9: Comparison between the current approach based on joint metamodeling and the approach introduced in [EAHL+20] combining metamodeling in the control space with quantization in the uncertain space. The costs induced by the initial designs (RLHD of size 9) are not compatibilized. The uncertainty is modelled by a Brownian motion.

m , that is to say with a rough truncation error, involves a larger bias. Nevertheless, refining the heteroscedastic noise estimation should bring the method to a similar level but much further on the axis corresponding to the number of simulations.

But on function 2 with a Max-stable process, the heteroscedastic model slightly outperforms the homoscedastic models ($m = 2, 4, 8$) when approaching the 150 simulations (Figure 10). We can understand this improvement by the fact that even with higher m a homoscedastic model does not make up for a wider truncation error which is better approximated by a heteroscedastic model. Note that it is possible to relax the "nearly Gaussian" hypothesis on \mathbf{V} . In that case the same kind

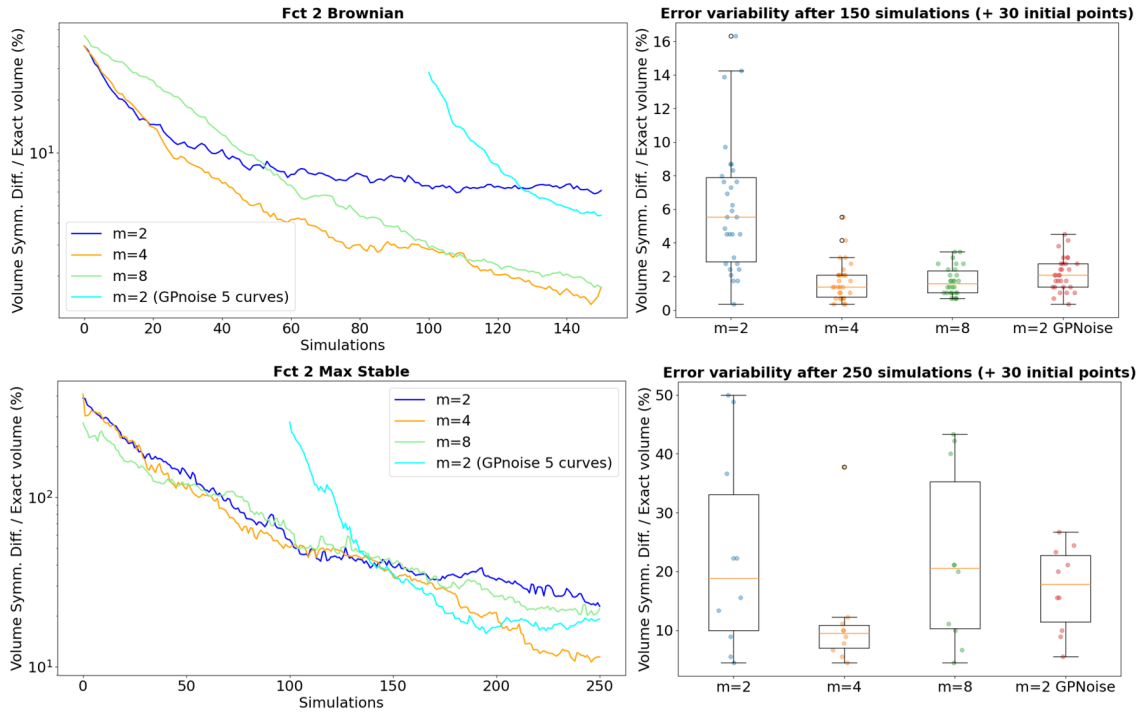


Figure 10: Function 2 with Brownian (top) and max-stable processes (bottom) with a comparison with the heteroscedastic GP model. Convergence of Algorithm 1 for $m = \{2, 4, 8\}$. Left: mean of the symmetric difference vs. number of simulator calls. The mean is taken over the independent runs of initial RLHD. The additional curve (cyan) corresponds to $m = 2$ with the heteroscedastic model, it is translated to take into account the extra-cost of 100 simulations for the noise estimation. Right: symmetric differences associated with the random initial DoEs at the maximal simulation budget.

of heteroscedastic variance estimator could be used but would require an empirical estimation of the conditional distribution of $\tilde{\mathbf{U}}|\mathbf{U}$ which seems difficult in the context of our partial knowledge of \mathbf{V} imposing on us to work on finite predefined sets \mathcal{G} and $\tilde{\mathcal{G}}_{m,L}$.

4.4. Application to a pollution control system SCR

In this section we test the proposed method on an automotive test case from IFPEN. The problem concerns an after-treatment device of diesel vehicles, called Selective Catalytic Reduction (SCR). This latter consists of a basic process of chemical reduction of nitrogen oxides (NOx) to diatomic nitrogen (N₂) and water (H₂O) by the reaction of NOx and ammonia NH₃. The reaction itself occurs in the SCR catalyst. Ammonia is provided by a liquid-reductant agent injected upstream of the SCR catalyst. The amount of ammonia introduced into the reactor is a critical quantity: overdosing causes undesirable ammonia slip downstream of the catalyst, whereas underdosing causes insufficient NOx reduction. In practice, ammonia slip is restricted to a prescribed threshold. We use an emission-oriented simulator developed by IFPEN, which models the vehicle, its engine and the exhaust after-treatment system. This latter takes as input the vehicle driving cycle profile and provides the time-series of corresponding exhaust emissions as output. A realistic SCR control law is used in this simulator. See [BCLP12] for an example of such a control law. In this study, the inputs are two control variables and a functional one considered as random. The control variables are parameters of the SCR control law. They set the targeted level of NH₃ storage in the catalyst and then are indirectly related to the NH₃ injected. They lie in $\mathbb{X} = [0, 0.6]^2$. The functional random variable describes the evolution of vehicle speed on $I = [0, 5400\text{s}]$ and is known through an available sample of 100 real driving cycles. A few samples are represented in Figure 11. In short, the ammonia emissions peak during a driving cycle is modelled as a function

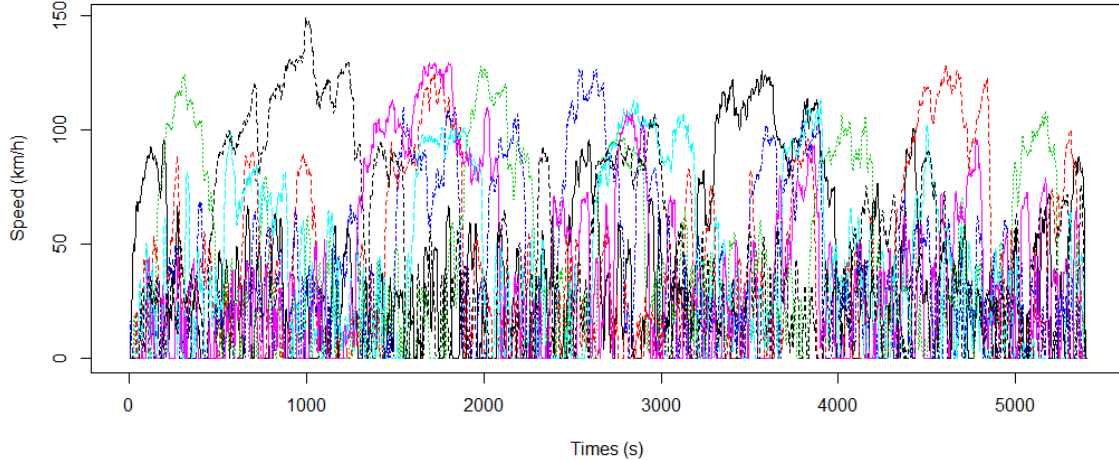


Figure 11: Seven real-driving cycles extracted from the available sample of 100 cycles.

$$f : \begin{cases} \mathbb{X} \times \mathcal{V} & \rightarrow \mathbb{R} \\ (\mathbf{x}, \mathbf{V}) & \mapsto f(\mathbf{x}, \mathbf{V}) = \max_{t \in I} NH_3^{slip}(t) \end{cases} \quad (16)$$

We are interested in recovering the set $\Gamma^* = \{\mathbf{x} \in \mathbb{X}, g(\mathbf{x}) = \mathbb{E}_{\mathbf{V}}[f(\mathbf{x}, \mathbf{V})] \leq c\}$, with $c = 30\text{ppm}$. Conducting this study on a full grid would consist in covering the space $[0, 0.6]^2$ with a fine mesh and evaluating the code 100 times at each point. Knowing that each simulation takes about two minutes, such study would require many hours of computational time, and thus using

meta-models allows to tackle this computational issue.

As discussed in the previous subsection, we start by reducing the space dimension of the uncertain variable as described in Section 2.1 and fix the truncation argument to $m = 20$ in order to explain 80% of the variance. Thereafter, we consider a Gaussian Process prior $Z_{(\mathbf{x}, \mathbf{u})}$, with constant mean function and Matérn covariance kernel with $\nu = 5/2$. The initial DoE consists of a $n = 5 \times (2 + 20) = 110$ points LHS design optimized with respect to the maximin criterion. The covariance kernel hyper-parameters are estimated by maximizing the likelihood. As for the analytical example, we proceed to add one point at each iteration of the SUR strategy.

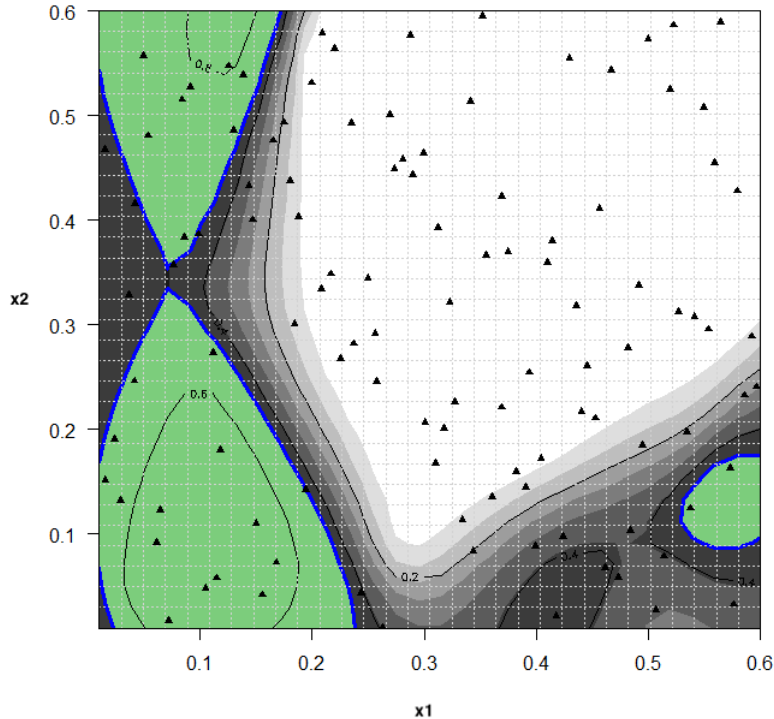


Figure 12: SCR pollution control system. The initial DoE (black triangles) and the initial estimate set (green). The contour plot in grey represents the excursion probability.

Figure 12 shows the coverage probability function defined by the integrated Gaussian Process $Y_{\mathbf{x}}$ conditionally to the n available observations. The initial estimate of Γ^* is given by the green set of blue boundary. From Figure 13, we note that, for each additional point, the new observed response affects the estimation of the excursion set and its uncertainty. Thus, the Vorob'ev deviation generally decreases in function of the iterations. SUR algorithm heavily visits the boundary region of Γ^* and explore also other potentially interesting regions. Actually, after 400 iterations (510 evaluations) the whole domain \mathbb{X} has an excursion probability close to either 0 or 1.

5. Conclusion and extension

The aim of this paper is to propose an excursion set inversion procedure for control system in an uncertain environment. Furthermore, control systems whose behaviour is simulated by high-fidelity and expensive-to-evaluate models are considered. Gaussian Process modelling approaches are therefore introduced as computationally costless approximations of the outputs of the simulator.

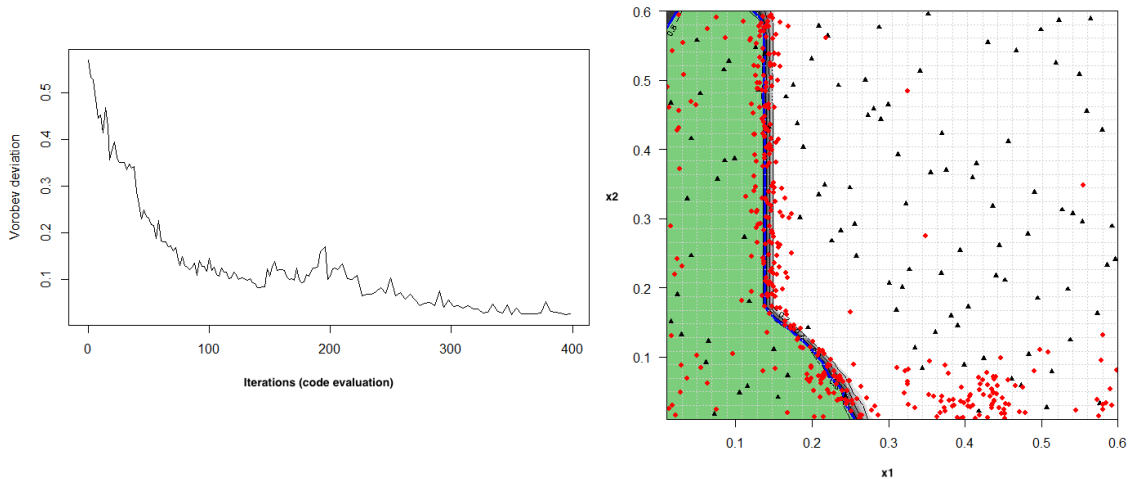


Figure 13: SCR pollution control system. The Vorob'ev deviation in function of the number of simulations (left). The coverage probability function, the initial DoE (black triangles) and the estimate set (green set) after 400 added points (red). The contour plot in grey represents the excursion probability.

The proposed strategy minimizes the uncertainties on the excursion set of the simulator output by, first, creating a Gaussian Process model in the joint space of deterministic and uncertain input variables. The vector-valued random variables result from a dimension reduction of the functional input variable. Then another "projected" Gaussian Process is built to represent the mean of the quantity of interest (output of the simulator). Enrichment of the design of experiments is performed in the joint space. This allows us to guide the experimental design points toward regions of the space that decrease significantly the uncertainties on the excursion set while limiting the number of simulations.

Two bi-dimensional examples based on analytic expressions are considered to validate the proposed procedure. This allows us to validate the proposed method with comparison with exact solutions. The application of the proposed procedure shows increased efficiency as the number of calls to the complex simulator is reduced. Finally, we apply the methodology to an industrial problem related to the pollution control system of an automotive. An excursion set solution is found within a reasonable number of simulations.

The paper focuses on the expectation while other reliability measures may also be of great importance. For example, one may be interested in ensuring a certain level of reliability with a high probability or satisfying multiple constraints, e.g., on the mean and the variance.

One limitation of our methodology is the prior choice of the truncation argument m . It can be based on a sufficient level of explained variance. But, depending on the stochastic process involved, this parameter can be high (8 for the Max-stable process on analytical function 2, 20 for the industrial application). Increasing m implies increasing the dimension of the GP space. A high number of design points is then needed to produce an accurate response surface, which is very costly in simulation calls. To overcome this, another variant of our strategy can be studied. The approach consists in augmenting the uncertain space sequentially when needed. More precisely, a first Gaussian Process is defined in the $p + m$ dimensional space, with m chosen small. Once the enrichment strategy (given by Algorithm 1) no longer provides information - a rough approximation of the excursion set is achieved - the dimension of the uncertain space is increased and the GP is updated in the $p + m + 1$ dimensional space. It is important to underline that this approach does not require additional calls to the numerical simulator. This alternative strategy is summarized by Algorithm 2:

Algorithm 2 Stochastic inversion via sequential joint space modelling

Require: The initial truncation argument $m = 2$ and the DoE of n points $\mathcal{X}_n \times \mathcal{U}_n$ in $(\mathbb{X}, \mathcal{G}_m)$

- 1: Set $n = n_0$.
 - 2: Calculate \mathbf{Z} the simulator responses at the design points $\mathcal{X}_n \times \mathcal{U}_n$
 - 3: **while** $n \leq \text{budget}$ **do**
 - 4: $m \leftarrow \text{Update.Dimension}()$
 - 5: Fit the GP model Z^n
 - 6: Induce the integrated GP $Y_{\mathbf{x}}^n$
 - 7: $\mathbf{x}_{n+1} \leftarrow \text{sampling criterion } \mathcal{J}_n$
 - 8: $\mathbf{u}_{n+1} \leftarrow \arg \min_{\mathbf{u} \in \mathcal{G}} \text{VAR}(Y_{\mathbf{x}_{n+1}}^{n+1})$
 - 9: Simulator response at $(\mathbf{x}_{n+1}, \mathbf{v}_{n+1})$, where $\mathbf{v}_{n+1} \in \Xi$ is the curve corresponding to \mathbf{u}_{n+1}
 - 10: Update DoE : $\mathcal{X}_{n+1} \times \mathcal{U}_{n+1} = \mathcal{X}_n \times \mathcal{U}_n \cup \{(\mathbf{x}_{n+1}, \mathbf{v}_{n+1})\}$
 - 11: Update $\mathbf{Z} = \mathbf{Z} \cup \{f(\mathbf{x}_{n+1}, \mathbf{v}_{n+1})\}$
 - 12: Set $n = n + 1$
 - 13: **end while**
 - 14: Fit the GP model Z^n
 - 15: Approximate Γ^* by the Vorob'ev expectation
-

In **step** 4 of Algorithm 2, the uncertain space dimension is updated based on a stagnation criterion of the Vorob'ev Deviation (see Eq.(26) in [EAHL⁺20]). If the criterion is verified then one dimension is added and thus $m = m + 1$.

This strategy, based on an adaptive choice of m presented in Algorithm 2, has been evaluated on the second analytical function of Section 4.1. A small initial value of m is chosen, $m = 2$, and it is then increased when the variation of the Vorob'ev deviation remains smaller than a given threshold ϵ (0.005) during l_0 consecutive iterations ($l_0 = 4$) (see Eq. (26) in [EAHL⁺20]). It allows to increase the dimension of the KL reduced space only when it is necessary to obtain a better accuracy. As illustrated on Figure 14 it allows to save simulations and reduce computational time. The accuracy reached with this strategy is similar to the one obtained with the strategy with fixed $m = 8$ but with a gain of $\approx 12\%$ in terms of computational time (Figure 15). The first iterations are performed with $m = 2$, only the last iterations are performed with $m = 8$.

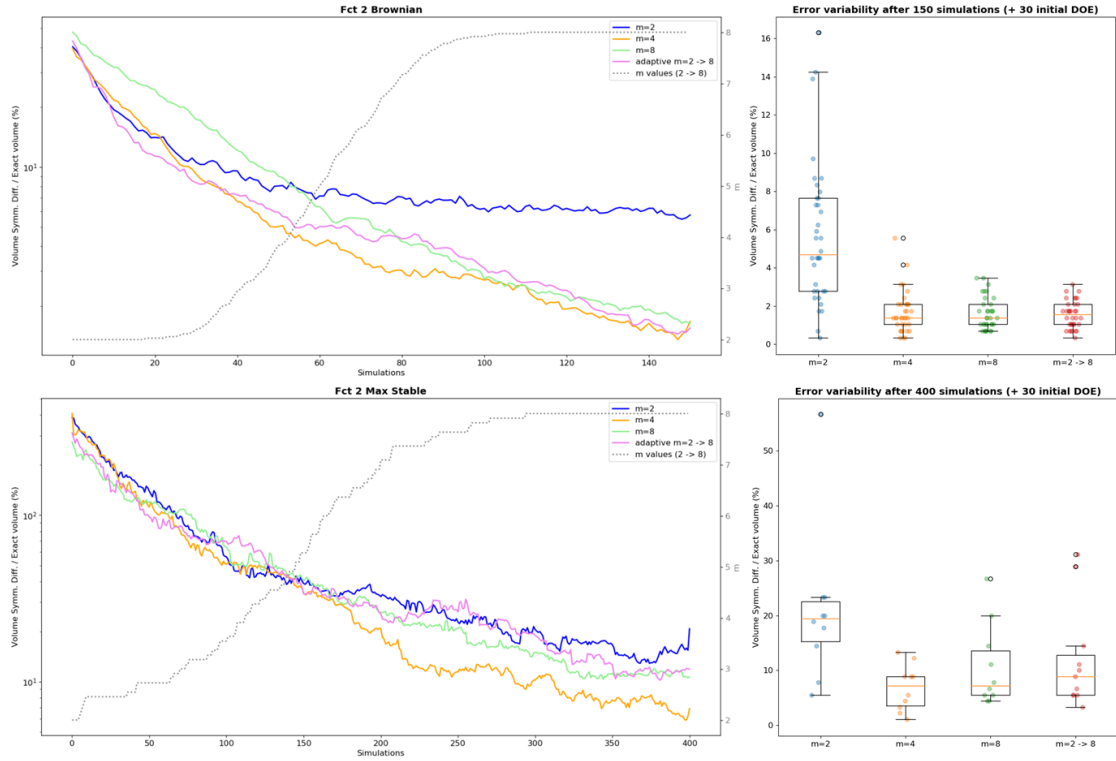


Figure 14: Analytical example 2 with Brownian motion (top) and with max-stable process (bottom). Convergence of Algorithm 1 for $m = \{2, 4, 8\}$ and for adaptive choice of m value. Left: mean of the symmetric differences vs. number of simulator calls in log scale. The dashed grey curve is the mean of m values in the case of an adaptive choice of its value. The mean is taken over the independent runs of initial RLHD. Right: symmetric differences associated with the random initial DoEs at the maximal simulation budget.

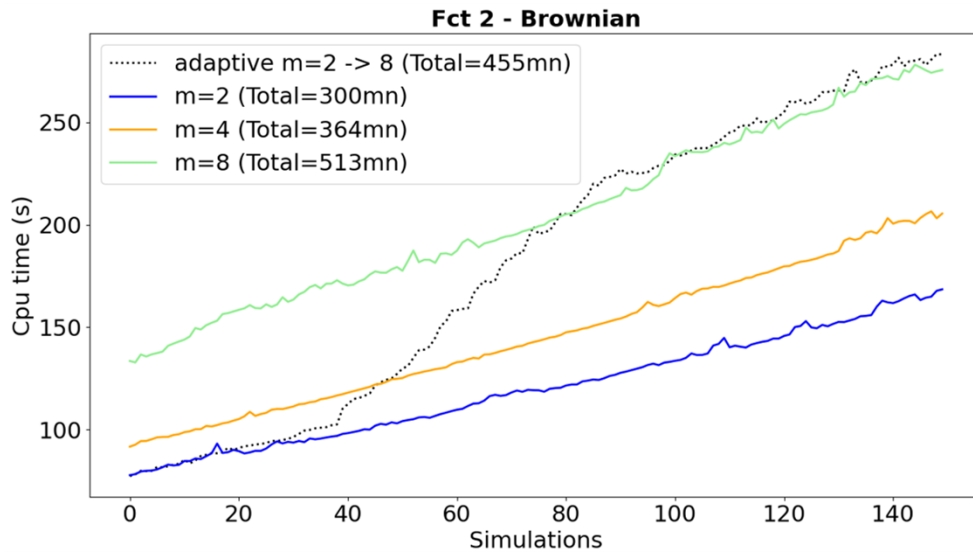


Figure 15: The computational time (sec.) needed to provide the next evaluation point as a function of iterations for the second analytic example with Brownian motion. The values are averaged computational times for 5 runs of each strategy: $m = 2, 4, 8$ and adaptive choice of m value.

References

- [Adl81] Robert J. Adler. *The Geometry of Random Fields*. John Wiley & Sons, Chichester, 1981.
- [BCLP12] Anthony Bonfils, Yann Creff, Olivier Lepreux, and Nicolas Petit. Closed-loop control of a scr system using a nox sensor cross-sensitive to nh3. *IFAC Proceedings Volumes*, 45(15):738–743, 2012.
- [BGL⁺12] Julien Bect, David Ginsbourger, Ling Li, Victor Picheny, and Emmanuel Vazquez. Sequential design of computer experiments for the estimation of a probability of failure. *Statistics and Computing*, 22(3):773–793, 2012.
- [BL15] David Bolin and Finn Lindgren. Excursion and contour uncertainty regions for latent gaussian models. *Journal of the Royal Statistical Society: Series B (Statistical Methodology)*, 77(1):85–106, 2015.
- [CBG⁺14] Clément Chevalier, Julien Bect, David Ginsbourger, Emmanuel Vazquez, Victor Picheny, and Yann Richet. Fast parallel kriging-based stepwise uncertainty reduction with application to the identification of an excursion set. *Technometrics*, 56(4):455–465, 2014.
- [CG13] Clément Chevalier and David Ginsbourger. Fast computation of the multi-points expected improvement with applications in batch selection. In *International Conference on Learning and Intelligent Optimization*, pages 59–69. Springer, 2013.
- [Doo53] Joseph Leo Doob. *Stochastic processes*. New York: John Wiley & Sons, 1953.
- [EAHL⁺20] Mohamed Reda El Amri, Céline Helbert, Olivier Lepreux, Miguel Munoz Zuniga, Clémentine Prieur, and Delphine Sinoquet. Data-driven stochastic inversion via functional quantization. *Statistics and Computing*, 30(3):525–541, 2020.
- [FS⁺13] Joshua P French, Stephan R Sain, et al. Spatio-temporal exceedance locations and confidence regions. *The Annals of Applied Statistics*, 7(3):1421–1449, 2013.
- [JLR13] Janis Janusevskis and Rodolphe Le Riche. Simultaneous kriging-based estimation and optimization of mean response. *Journal of Global Optimization*, 55(2):313–336, 2013.
- [JS11] Walter Mebane Jr. and Jasjeet Sekhon. Genetic optimization using derivatives: The rgenoud package for r. *Journal of Statistical Software*, 42(11):1–26, 2011.
- [LK10] Olivier Le Maître and Omar M. Knio. *Spectral Methods for Uncertainty Quantification*. Scientific Computation. Springer, Dordrecht, 2010.
- [Mol06] Ilya Molchanov. *Theory of random sets*. Springer Science & Business Media, 2006.
- [Pac03] Christopher Joseph Paciorek. *Nonstationary Gaussian processes for regression and spatial modelling*. PhD thesis, Department of Statistics, Carnegie Mellon, University Pittsburgh Pennsylvania 15213, 2003.
- [RGD12] Olivier Roustant, David Ginsbourger, and Yves Deville. Dicekriging, diceoptim: Two r packages for the analysis of computer experiments by kriging-based metamodeling and optimization. *Journal of Statistical Software*, 51(1):1–55, 2012.
- [VB09] Emmanuel Vazquez and Julien Bect. A sequential bayesian algorithm to estimate a probability of failure. *IFAC Proceedings Volumes*, 42(10):546–550, 2009.

- [VL13] Oleg Yu. Vorobyev and Natalia A. Lukyanova. A mean probability event for a set of events. Mpra paper, University Library of Munich, Germany, 2013.
- [Vor84] O Yu Vorob'ev. Srednemernoje modelirovanie (mean-measure modelling), 1984.
- [WSN00] Brian J Williams, Thomas J Santner, and William I Notz. Sequential design of computer experiments to minimize integrated response functions. *Statistica Sinica*, pages 1133–1152, 2000.